Electron-impact study of the O_2 molecule using the *R*-matrix method

Jasmeet Singh* and K. L. Baluja†
Department of Physics and Astrophysics, University of Delhi, Delhi-110007, India
(Received 23 June 2014; published 25 August 2014)

We have computed elastic differential, momentum-transfer, excitation, ionization cross sections, collision frequencies, and scattering length for electron impact on the O_2 molecule, which are computed using the *R*-matrix method. The results of the static exchange, correlated one-state, and 22-state close-coupling approximation are presented. We have detected a stable anionic bound state $^2\Pi_g$ of O_2^- and two shape resonances of $^2\Pi_u$ symmetry. The dissociative nature of these shape resonances is explored by performing scattering calculations in which the O-O bond is stretched. These resonances support dissociative attachment yielding O, O^- in dissociation of O_2. Born correction is applied for higher partial waves neglected in the *R*-matrix calculations for elastic and dipole allowed transitions.

DOI: 10.1103/PhysRevA.90.022714 PACS number(s): 34.80.Bm, 34.80.Gs, 34.80.Ht

I. INTRODUCTION

Molecular oxygen plays a fundamental role in the physics and chemistry of the earth's atmosphere [1]. Detailed information about collisions between low-energy electrons and oxygen molecules is required in studies of the physics of planetary atmosphere, gaseous discharges, and both astrophysical and laboratory plasmas [2]. It is the electronic transition from the $X\,^3\Sigma_g^-$ state of oxygen to the $a\,^1\Delta_g$ and $b\,^1\Sigma_g^+$ states that give rise to the infrared and red bands in the atmospheric spectrum. The long lifetime of the metastable state ($a\,^1\Delta_g$) of oxygen makes scattering from an excited molecular target state possible [3]. The best known example of a $^3\Sigma_g^-$-$^3\Sigma_u^-$ transition for identical nuclei [4] is the ultraviolet absorption band system of O_2. In both O_2 and S_2 bands the even-numbered rotational lines are missing [4]. The O and S nuclei follow Bose statistics, the lower states, that is the ground states of the O_2 and S_2 molecules, must be $^3\Sigma_g^-$.

The valence configuration interaction (VCI) and self-consistent field (SCF) results of O_2 and S_2 were obtained by Tait *et al.* [5] using an identical minimal basis set composed of Slater-type orbitals. Moss *et al.* [6] reported configuration interaction calculations as a function of internuclear distance for nine states of O_2, i.e., $X\,^3\Sigma_g^-$, $a\,^1\Delta_g$, $b\,^1\Sigma_g^+$, $c\,^1\Sigma_u^-$, $C\,^3\Delta_u$, $A\,^3\Sigma_u^+$, $B\,^3\Sigma_u^-$, $^1\Delta_u$, $^1\Sigma_u^+$, by using the generalized valence bond (GVB) orbitals of the ground state. Previous theoretical investigation of the spectrum of O_2 include two minimal Slater basis sets, and complete valence CI calculations by Beebe *et al.* [7]. Saxon and Liu [8] performed configuration interaction calculations using an extended one-particle basis set, and included internal and semi-internal electron correlation effects. A multichannel effective range theory (ERT) of the electron impact electronic excitation via a shape resonance was applied [9] to the excitation of the $a\,^1\Delta_g$ and $b\,^1\Sigma_g^+$ states of O_2 through the $O_2^-(^2\Pi_g)$ shape resonance. Noble and Burke [10] reported a nine-state *R*-matrix calculation of integral cross sections (ICSs) for elastic scattering of electrons by molecular oxygen. Their work was followed by Higgins *et al.* [11] in which they adopted the Born-Oppenheimer approximation in which the nuclear and electronic motions are treated separately. They consider several internuclear separations for the O_2 molecule to determine the effect on the cross sections. Machado *et al.* [12] used a combination of the Schwinger variational iterative method and the distorted-wave approximation to study elastic electron scattering by O_2 for incident energies ranging from 5–500 eV. They reported differential, integral, and momentum transfer cross sections. Theoretical studies on electron scattering and ionization of ozone, atomic, and molecular oxygen, and O_4 were done by Joshipura *et al.* [13], using complex scattering potential-ionization contribution method in which a complex energy-dependent potential derived from the atomic/molecular electron charge density. The ionization cross-section data for electron impact on O_2, for energy range from threshold to 1000 eV, were generated experimentally [14] using a crossed electron-molecular beam collision geometry and relative flow technique. Experimental and theoretical differential cross sections for the electron impact excitation of the $a\,^1\Delta_g$ and $b\,^1\Sigma_g^+$ electronic states of O_2 were determined [2] at different energies ranging from 5–20 eV. Differential and integral cross sections for elastic scattering of low-energy electrons by O_2 were reported by Sullivan *et al.* [15]. Woste *et al.* [16] measured relative angular distributions between 5 and 20 eV and then placed them on an absolute scale by normalization at a scattering angle of 60° where DCS of Shyn and Sharp [17] and Sullivan *et al.* [15] agreed. For electron scattering angles of less than 60°, there is a quite serious discrepancy in the literature between the DCS measurements of Woste *et al.* [16] and Sullivan *et al.* [15]. Green *et al.* [18] developed and applied, experimentally, the relative flow technique to determine DCS for electron scattering by O_2. They found that at each of three energies (5, 7, and 10 eV) the present DCS results were in excellent agreement with those of Sullivan *et al.* Their work resolved the discrepancy in the DCS, for energies in the range 5–10 eV, between Sullivan *et al.* [15] and the earlier measurements in favor of Sullivan *et al.*

The main motivation of the present work is to improve the polarization effect by including many excited states in the trial wave function of the entire scattering system, and compare with the previous work. The effect of the enhanced polarization is studied on the well-known shape resonances of *a* and *b* states of O_2 and their effect on the dissociation electron attachment process.

*Also at Keshav Mahavidyalaya, Department of Physics, University of Delhi, Delhi-110034, India; rajvanshi_jasmeet@yahoo.co.in
†kl_baluja@yahoo.com

The present study uses the *ab initio* *R*-matrix method to low-energy scattering of the O_2 molecule in the fixed nuclei approximation. The calculations use the UK molecular *R*-matrix code [19,20]. The *R*-matrix method has the advantage over other scattering methods in providing cross sections at a large number of scattering energies efficiently. It also has the ability to include correlation effects and give an adequate representation of several excited states of the molecule [21]. We are interested in the low-energy region ($\leqslant$10 eV), which is a favorite ground for the *R*-matrix method. The incoming electron can occupy one of the many unoccupied molecular orbitals or can excite any of the occupied molecular orbitals as it falls into another one. These processes give rise to the phenomenon of resonances forming a negative molecular ion for a finite time before the resonance decays into energetically open channels.

Electron scattering calculations are performed at static exchange, one-state CI, and close-coupling approximation in which we have retained twenty target states in the *R*-matrix formalism. The integrated elastic, the differential, and momentum cross sections for electron impact on the O_2 molecule from its ground state are reported. The excitation cross sections from the ground state to few low-lying excited states have also been calculated. We have also computed the binary-encounter-Bethe (BEB) ionization cross section [22,23]. The BEB cross sections depend only on the binding energies, kinetic energies, and the occupation number of the occupied molecular orbitals of the target, and on the energy of the incident electron. The momentum transfer cross sections calculated in the *R*-matrix approximation have been used to calculate effective collision frequency over a wide electron temperature range. We have also evaluated scattering length of the O_2 molecule.

II. METHOD

Since the *R*-matrix theory has been described in detail elsewhere [24–27], we only give an outline here. In an *R*-matrix approach, there are two distinct physically separated spatial regions, an inner region and an outer region, that are defined with respect to electron-molecule distances. These are treated differently in accordance with the different forces operating in each region. When the scattering electron leaves the inner region, the other target electrons are confined to the inner region. Here the *R*-matrix boundary radius was chosen to be $10\,a_0$ centered at the center of mass of the O_2 molecule; the resulting sphere encloses the entire charge density of the molecule so that the amplitudes of the various occupied and virtual target orbitals are negligible at the boundary. However, the continuum orbitals have finite amplitudes at the boundary. In the present case, the target boundary amplitudes at $10\,a_0$ are less than $10^{-5}\ a_0^{-3/2}$ for the occupied and virtual orbitals. Inside the *R*-matrix sphere, the electron-electron correlation and exchange interactions are strong. Short-range correlation effects are important for accurate prediction of large-angle elastic scattering and exchange effects are important for spin-forbidden excitation cross sections.

A multicentered CI wave function expansion is used in the inner region. The calculation in the inner region is similar to a bound-state calculation, which involves the solution of an eigenvalue problem for $(N+1)$ electrons in the truncated space, where there are N target electrons and a single scattering electron. Outside the sphere, only long-range multipolar interactions between the scattering electron and the various target states are included. Since only direct potentials are involved in the outer region, a single center approach is used to describe the scattering electron via a set of coupled differential equations. The *R*-matrix is a bridge between the two regions. It describes how the scattering electron enters the inner region and how it leaves. In the outer region, the *R*-matrix on the boundary is propagated outwards [28,29] until the inner-region solutions can be matched with asymptotic solutions thus yielding the physical observables such as cross sections.

In the polyatomic implementation of the UK molecular *R*-matrix code [19,20], the continuum molecular orbitals are constructed from atomic Gaussian-type orbitals (GTOs) using basis functions centered on the center of gravity of the molecule. The main advantage of GTOs is that integrals involving them over all space can be evaluated analytically in closed form. However, a tail contribution is subtracted to yield the required integrals in the truncated space defined by the inner region [19].

The target molecular orbital space is divided into core (inactive), valence (active), and virtual orbitals. The target molecular orbitals are supplemented with a set of continuum orbitals, centered on the center of gravity of the molecule. The continuum basis functions used in polyatomic *R*-matrix calculations are Gaussian functions and do not require fixed boundary conditions. First, target and continuum molecular orbitals are orthogonalized using Schmidt orthogonalization. Then symmetric or Löwdin orthogonalization is used to orthogonalize the continuum molecular orbitals among themselves and remove linearly dependent functions [19,30]. In general and in this work, all calculations are performed within the fixed-nuclei approximation.

In the inner region, the wave function of the scattering system, consisting of target plus scattering electron, is written using the CI expression:

$$\Psi_k^{N+1} = A\sum_i \phi_i^N(x_1,\ldots,x_N)\sum_j \xi_j(x_{N+1})a_{ijk} + \sum_m \chi_m(x_1,\ldots,x_N,x_{N+1})b_{mk}, \quad (1)$$

where A is an antisymmetrization operator, x_N is the spatial and spin coordinates of the Nth electron, ϕ_i^N represents the ith state of the N-electron target, ξ_j is a continuum orbital spin-coupled with the scattering electron, and k refers to a particular *R*-matrix basis function. Coefficients a_{ijk} and b_{mk} are variational parameters determined as a result of the matrix diagonalization.

The first sum runs over the 22 target states of O_2 included in the present calculation, which are represented by a CI expansion. To obtain reliable results, it is important to maintain a balance between the N-electron target representation, ${\phi_i}^N$, and the $(N+1)$ electron-scattering wave function. The summation in the second term of Eq. (1) runs over configurations χ_m, where all electrons are placed in target-occupied and virtual molecular orbitals. The choice of appropriate χ_m is

crucial in this [31]. These are known as L^2 configurations and are needed to account for orthogonality relaxation and for correlation effects arising from virtual excitation to higher electronic states that are excluded in the first expansion. The basis for the continuum electron is parametrically dependent on the R-matrix radius and provides a good approximation to an equivalent basis of orthonormal spherical Bessel functions [32].

We have used 37 a_g, 19 b_{2u}, 19 b_{3u}, 16 b_{1g}, 21 b_{1u}, 17 b_{3g}, 17 b_{2g}, and 6 a_u continuum orbitals for O_2. The target and the continuum orbitals of a particular symmetry form an orthonormal set in the inner region, for example, the 3 a_g orbitals of the target and 37 a_g orbitals of the continuum are orthonormal to each other. The configuration state function (CSFs) in the second term in Eq. (1) were constructed by allowing the scattering electron to occupy any of the target occupied or virtual orbitals. This term is responsible for the polarization effects in the one-state CI calculation also.

III. RESULTS

A. Target and scattering model

The molecule O_2 is a linear open-shell system that has ground state $X\,^3\Sigma_g^-$ in the $D_{\infty h}$ point group which is reduced to the D_{2h} point group when the symmetry is lowered. The point group D_{2h} is the highest Abelian group in our codes. The results are reported in the natural symmetry point group as well as in the D_{2h} point group for the sake of convenience. We used a double ζ plus polarization (DZP) Gaussian basis set [33] contracted as (9,5,1)/(4,2,1) for O. We avoided using diffuse functions as these would extend outside the R-matrix box that may cause linear dependency problems. We first performed an SCF calculation for the ground state of the O_2 molecule with the chosen DZP basis set and obtained a set of occupied and virtual set of orbitals.

The Hartree-Fock electronic configuration for the ground state is $1\sigma_g^2$ - $3\sigma_g^2$ $1\sigma_u^2$ - $2\sigma_u^2$ $1\pi_u^4$ $1\pi_g^2$, which gives rise to the lowest-lying $X\,^3\Sigma_g^-$, $a\,^1\Delta_g$, and $b\,^1\Sigma_g^+$ states [4]. The energy of the occupied $1\pi_g$ orbital is -13.94 eV. In our limited CI model, we keep four electrons frozen in the $1\sigma_g^2\,1\sigma_u^2$ configuration and allow the remaining 12 electrons to move freely in molecular orbitals $2\sigma_g$, $3\sigma_g$, $2\sigma_u$, $3\sigma_u$, $1\pi_u$, and $1\pi_g$. The CI ground-state energy for the O_2 molecule is -149.6984 hartrees, at a bond length of $R_e = 2.42a_0$. We computed the value of vertical electronic affinity (VEA) by performing a bound-state calculation of O_2^- by including the continuum electron basis functions centered at the origin. The vertical electron affinity is equal to the difference in total energy of the neutral molecule and its anion at the equilibrium geometry of the neutral molecule. We detect a stable bound state of O_2^- with $^2\Pi_g$ symmetry having the configuration $1\sigma_g^2$ - $3\sigma_g^2$ $1\sigma_u^2$ - $2\sigma_u^2$ $1\pi_u^4$ $1\pi_g{}^3$ with a VEA value of 0.389 eV for O_2, which is in good agreement with theoretical value 0.390 eV [34] and experimental value of 0.451 ± 0.007 eV [35]. In our CI model the absolute values of quadrupole component Q_{20} for the ground state is 0.275 a.u.. The values of the ground-state energy and the rotational constant are compared with other work in Table I. In Table II, we list the quadrupole moment of each state (Q_{20}), N the number of CSFs, and the vertical excitation energies for the target states. We have reasonable agreement with the calculations of [2,6–9] for vertical excitation energies.

TABLE I. Properties of the O_2 target, ground-state energy (in a.u.), and the rotational constant (B_e, in cm^{-1}), SCF at bond length $R_e = 2.2\ a_0$ and CI at bond length $R_e = 2.42\ a_0$.

	Present work		Previous results[a]	
	SCF	CI	SCF ($R_e = 2.32a_0$)	CI ($R_e = 2.46a_0$)
E	−149.6360	−149.6984	−149.0915	−149.2157
B_e	1.55	1.28	1.40	1.24

[a]Ref. [5].

B. Elastic and inelastic total cross sections

In Figs. 1–3 we have shown the inelastic cross sections from the ground state to the three physical states, with vertical excitation thresholds along with their quadrupole moments, and the number of CSFs included in the CI expansion are given in Table II. In Figs. 1 and 2 we notice sharp peaks at 6.04 eV and 6.02 eV in the cross section of $X\,^3\Sigma_g^-$-$a\,^1\Delta_g$ and $X\,^3\Sigma_g^-$-$b\,^1\Sigma_g^+$ transitions respectively. These shape resonances belong to degenerate $(^2B_{2u}/^2B_{3u})^2\Pi_u$ symmetries. The resonance properties of these peaks are also given in Table III. In Figs. 1 and 2, we have compared our results with another R-matrix calculation [10]. In Figs. 1 and 2, the peaks (resonances) in the excitation cross sections are at lower energy and more shaper than observed by Noble and Burke [10]. Figure 3 depicts the excitation cross section for the optically allowed transition $X\,^3\Sigma_g^-$ ($X\,^3B_{1g}$)-$B\,^3\Sigma_u^-$ ($B\,^3A_u$) [4]. In our results the Born correction is applied for this dipole transition having transition moment 0.51 a.u. This takes care of the partial wave contribution ($l > 4$) to the scattering cross section in the R-matrix results.

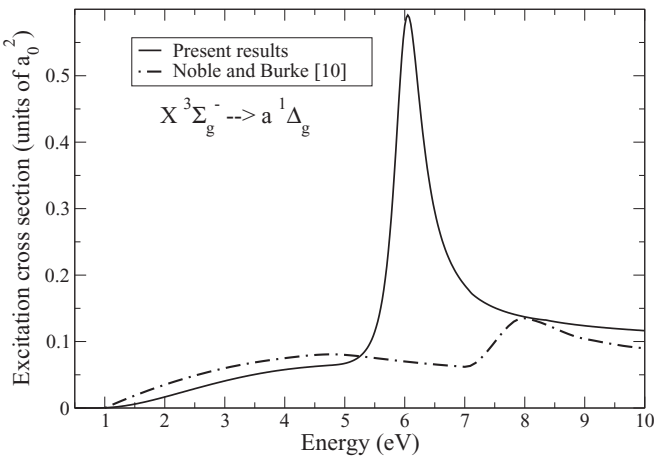

FIG. 1. Electron-impact excitation cross sections from the ground state: $X\,^3\Sigma_g^-$ ($^3B_{1g}$) of the O_2 molecule to the $a\,^1\Delta_g$ ($a\,^1A_g/^1B_{1g}$), solid line, present study; dash-dotted curve, Noble and Burke [10].

TABLE II. The vertical excitation energies (VEE in eV), quadrupole moments (Q_{20} in a.u.), and N the number of configuration state functions (CSFs) for the target states of O_2 at bond length $R_e = 2.42\ a_0$.

State $D_{2h}/D_{\infty h}$	Present (eV)	Ref. [2] (eV)	Ref. [9] (eV)	Ref. [8] (eV)	Ref. [7] (eV)	Ref. [6] (eV)	Q_{20} (a.u.)	N
$X\,^3B_{1g}/X\,^3\Sigma_g^-$	0.0	–	–	–	–		0.27	48
$a(^1A_g, {}^1B_{1g}/a\,^1\Delta_g$	0.85	0.93	0.98	1.09	0.92	1.08	0.29	60/36
$b(^1A_g)/b\,^1\Sigma^+{}_g$	1.31	1.47	1.65	1.77	1.36	1.69	0.31	60
$c(^1A_u)/c\,^1\Sigma_u^-$	4.54	5.49	6.12	3.88	3.05	3.93	0.88	36
$C(^3A_u, {}^3B_{1u})/C\,^3\Delta_u$	4.71	5.68	6.27	4.13	3.28	4.17	0.87	48/48
$A(^3B_{1u})/A\,^3\Sigma^+{}_u$	4.82	5.81	6.47	4.20	3.33	4.24	0.87	48
$^3B_{2g}, {}^3B_{3g}/{}^3\Pi_g$	7.10						1.32	48
$^1B_{2g}, {}^1B_{3g}/{}^1\Pi_g$	8.35			8.41	8.62		1.27	40
$1\ ^3B_{2u}, {}^3B_{3u}/1\ {}^3\Pi_u$	9.70						3.81	48
$B\,^3A_u/B\,^3\Sigma_u^-$	9.76	10.86	9.25	6.07	6.34	6.30	1.10	48
$^1B_{2u}, {}^1B_{3u}/{}^1\Pi_u$	10.97						3.74	40
$1\ (^1A_u, {}^1B_{1u})/1\ {}^1\Delta_u$	12.05	13.16	11.8	8.57	9.06	8.79	1.09	44/36
$1\ ^3B_{2u}, {}^3B_{3u}/1\ {}^3\Pi_u$	13.28						0.62	48
$(^1B_{1u})/{}^1\Sigma^+{}_u$	13.33	14.67	13.25	10.43	10.72	10.18	1.03	44

C. Dissociative electron attachment

The study of dissociative electron attachment (DEA) correlates various resonances to the possible reaction channels. In DEA experiments, the fragment negative ion yield is measured as a function of the kinetic energy of the incident electron. Due to the mechanism of resonant electron capture by the neutral molecule, a temporary negative ion is formed that may follow a dissociative decay channel, in which the negative ion so formed is sufficiently long lived that it can be directed to a mass filter. The molecule initially in the ground state makes a vertical transition to a repulsive electronic state of the scattering system through which it dissociates. The study of DEA provides an important input in the modeling of plasmas. It is also known that the secondary electrons cause damage to DNA via DEA. The present study identifies the presence of the bound state of $O_2{}^-$ in symmetry $^2\Pi_g$ ($^2B_{2g}/{}^2B_{3g}$) and shape resonance in $^2\Pi_u$ ($^2B_{2u}/{}^2B_{3u}$) symmetry. To explore the possible dissociative nature of this resonance state, we have investigated their dependence by stretching the O-O bond length from its equilibrium value to 3.5 a_0. This stretching mode asymptotically correlates to the following two-body fragmentation channel:

$$O_2{}^-(^2\Pi_u) \rightarrow O(^3P) + O^-(^2P^0). \quad (2)$$

In Fig. 4, we have shown the resonance position and the resonance width as a function of stretching bond O-O in D_{2h} symmetry for $^2\Pi_u$ ($^2B_{2u}/{}^2B_{3u}$). From Fig. 4 we observed that the resonance width and position decrease with increase in bond length of the O-O bond and they approach zero at 3.3 a_0; beyond this the resonance width and position vanish, which implies that these resonances become bound and support dissociative electron attachment. The variation of position and width of the $^2\Pi_u$ resonance with respect to the energy of the ground state as a function of internuclear distance is shown in Table IV. These data are useful to find DEA cross sections.

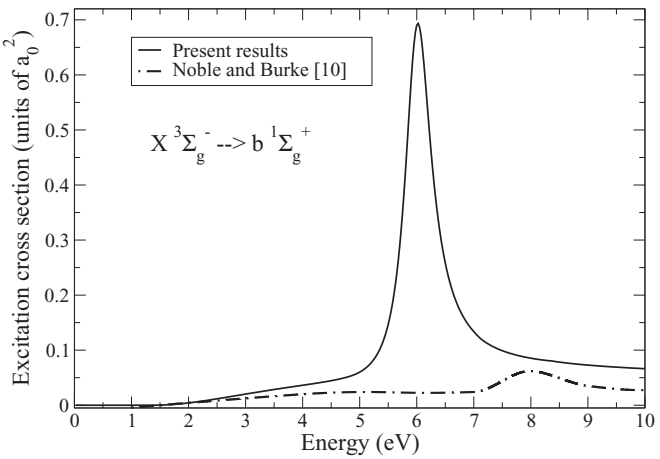

FIG. 2. Electron-impact excitation cross sections from the ground state: $X\,^3\Sigma_g^-$ ($^3B_{1g}$) of the O_2 molecule to the $b\,^1\Sigma_g^+$ ($b\,^1A_g$), solid line, present study; dash-dotted curve, Noble and Burke [10].

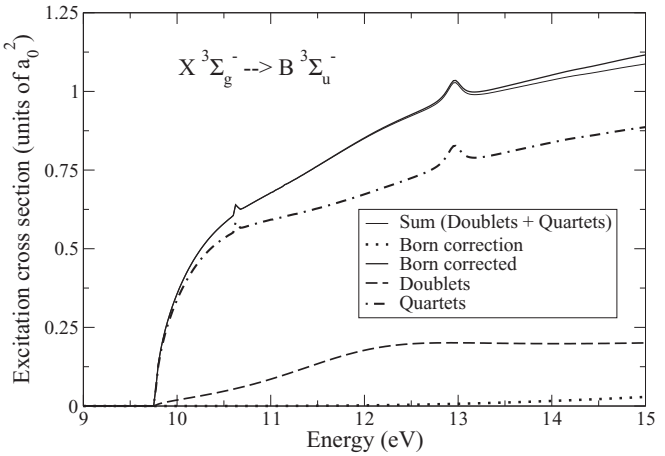

FIG. 3. Electron-impact excitation cross sections from the ground $X\,^3\Sigma_g^-$ ($^3B_{1g}$) state of the O_2 molecule to the $B\,^3\Sigma_u^-$ (^3A_u) state for 22 states calculation; dash-dotted curve, quartets; dashed curve, doublets; thin solid line, total sum (doublets + quartets); dotted curve, Born correction; thick solid line, Born corrected (sum of doublets, quartets and Born correction).

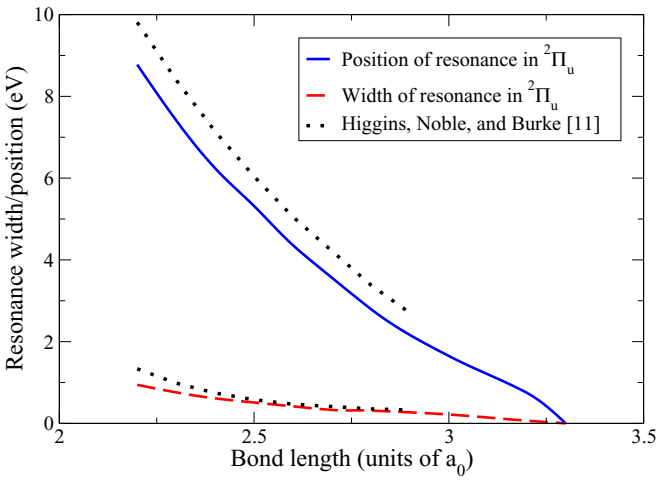

FIG. 4. (Color online) Variation of resonance width and position with bond length; solid blue curve, position of resonance ($^2\Pi_u$); dashed red curve, width of resonance ($^2\Pi_u$); dotted black curve, Higgins *et al.* [11].

D. Ionization cross section

Figure 5 shows electron-impact ionization cross section of O_2 from threshold 13.94 eV to 5000 eV by using the standard formalism of the BEB model [22,23]. This formalism requires the binding energy and kinetic energy of each occupied orbital in a molecular structure calculation. The ionization cross section rises from threshold to a peak value of 2.43×10^{-16}cm^2 at 114.72 eV and then shows $\ln(E/E)$ behavior as E approaches higher values. We have also shown the results of previous theoretical works [36] and [13], and experimental data by Krishnakumar *et al.* [14]. The molecular orbital data used in the calculation of BEB cross sections is given in Table V, which is generated at the SCF level.

The BEB ionization cross section σ is obtained by summing over each orbital cross section σ_i, where

$$\sigma_i(t) = \frac{s}{t+u+1}\left[\frac{1}{2}\left(1-\frac{1}{t^2}\right)\ln t + \left(1-\frac{1}{t}\right) - \frac{\ln t}{t+1}\right], \tag{3}$$

where $t = T/B$, $u = U/B$, and $s = 4\pi {a_0}^2 N(R/B)^2$. Here, R is the Rydberg energy, T is the kinetic energy of the incident electron, U is the orbital kinetic energy, N is the electron occupation number, and B is the binding energy of the orbital.

E. Differential cross section

The evaluation of the differential cross sections (DCS) provides a more stringent test for any theoretical model. The rotational excitation cross sections for electron impact on a neutral molecule can be calculated from the scattering parameters of elastic scattering in the fixed nuclei approximation provided the nuclei are assumed to be of infinite masses [37]. In particular, starting from an initial rotor state $J = 0$, the sum of all transitions from $J = 0$ level to a high enough J value for convergence is equivalent to the elastic cross section in the fixed nuclei approach. We have employed this methodology to extract rotationally elastic and rotationally inelastic cross sections from the K-matrix elements calculated in the one-state R-matrix model. The DCS for a general polyatomic molecule is given by the familiar expression

$$\frac{d\sigma}{d\Omega} = \sum_L A_L P_L(\cos\theta), \tag{4}$$

where P_L is a Legendre polynomial of order L. The a_L coefficients have already been discussed in detail [38]. For a polar molecule this expansion over L converges slowly. To circumvent this problem, we use the closure formula

$$\frac{d\sigma}{d\Omega} = \frac{d\sigma^B}{d\Omega} + \sum_L \left(A_L - A_L^B\right) P_L(\cos\theta). \tag{5}$$

The superscript B denotes that the relevant quantity is calculated in the Born approximation with an electron-point dipole interaction. The convergence of the series is now rapid since the contribution from the higher partial waves to the DCS is dominated by the electron-dipole interaction. The quantity $\frac{d\sigma}{d\Omega}$ for any initial rotor state $|Jm\rangle$ is given by the sum over all final rotor states $|J'm'\rangle$

$$\frac{d\sigma}{d\Omega} = \sum_{J'm'} \frac{d\sigma}{d\Omega}(Jm \to J'm'), \tag{6}$$

where J is the rotational angular momentum and m is its projection on the internuclear axis. To obtain converged results, the maximum value of $J' = 5$. We have calculated DCS by using the POLYDCS program of Sanna and Gianturco [39]

TABLE IV. Position and width of the $^2\Pi_u$ resonance with respect to the energy of the ground state as a function of internuclear distance, R (a_0).

R (units of a_0)	Position (E_r) (eV)	Width Γ_r (eV)
2.2	9.81	1.335
2.3	8.40	0.984
2.4	7.14	0.743
2.5	6.04	0.578
2.6	5.05	0.470
2.8	3.38	0.353
2.9	2.70	0.326

TABLE III. Resonance properties of O_2 at bond length $R = 2.42a_0$.

Electronic configuration of resonant state	E_r Resonance position (eV)	Γ_r Resonance width (eV)	Type of resonance	Parent state
$1\sigma_g^2 - 3\sigma_g^2 1\sigma_u^2 - 2\sigma_u^2 1\pi_u^4 1\pi_g\ ^3$: $^2\Pi_u$	6.04	0.89	Shape	$a\ ^1\Delta_g$
$1\sigma_g^2 - 3\sigma_g^2 1\sigma_u^2 - 2\sigma_u^2 1\pi_u^4 1\pi_g\ ^3$: $^2\Pi_u$	6.02	0.55	Shape	$b\ ^1\Sigma_g^+$

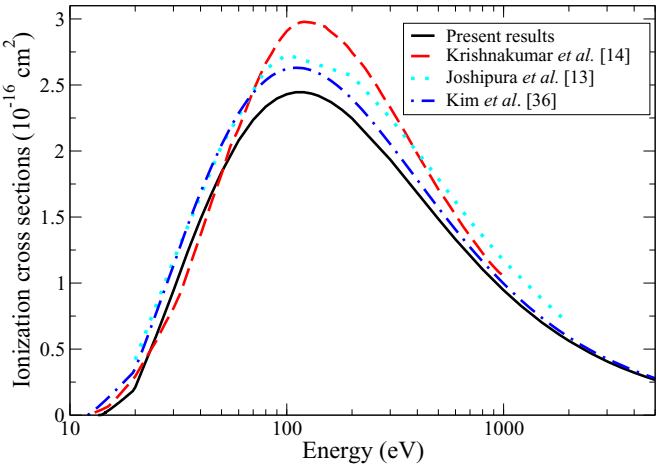

FIG. 5. (Color online) Electron-impact BEB ionization cross sections of the O_2 molecule; dashed red curve, Krishnakumar *et al.* (expt.) [14]; dotted cyan curve, Joshipura *et al.* (theoretical) [13]; dash-dotted blue curve, Kim *et al.* [36]; thick solid black line, our BEB model.

that requires basic molecular input parameters along with K matrices evaluated in a particular scattering calculation. We have used this code to compute the DCS in the one-state CI model. Since O_2 is an open-shell molecule having $X\,^3\Sigma_g^-$ as its ground state, the spin coupling between this target state and the spin of the incoming electron allows two spin-specific channels, namely the doublets (D) and quartets (Q) couplings. The spin-averaged DCS for elastic electron scattering from the O_2 molecule are calculated by using the statistical weight $2/6$ for doublets and $4/6$ for quartets scattering channels. We then use Eq. (3) as follows to calculate DCS:

$$\frac{d\sigma}{d\Omega} = \frac{1}{3}\left[2\left(\frac{d\sigma}{d\Omega}\right)^{Q} + \left(\frac{d\sigma}{d\Omega}\right)^{D}\right], \tag{7}$$

where $(\frac{d\sigma}{d\Omega})^{Q,D}$ represent DCS for quartet and doublet cases respectively.

In Fig. 6, we have shown the spin-averaged DCS calculated in the one-state R-matrix model at different energies. We have compared our results with the previous calculations [12,15,17,18].

TABLE V. O_2 molecular orbital binding and average kinetic energies for DZP basis set at equilibrium geometry. $|B|$ is binding energy, U is kinetic energy, and N is occupation number.

Molecular orbital	Our results $\|B\|$ (eV)	U (eV)	N
$1\sigma_g(1a_g)$	−563.82	794.49	2
$1\sigma_u(1b_{1u})$	−563.79	794.81	2
$2\sigma_g(2a_g)$	−46.03	79.86	2
$2\sigma_u(2b_{1u})$	−29.39	89.52	2
$3\sigma_g(3a_g)$	−20.23	73.16	2
$1\pi_u(1b_{2u})$	−19.66	60.57	2
$1\pi_u(1b_{3u})$	−19.66	60.57	2
$1\pi_g(1b_{3g})$	−6.97	82.85	1
$1\pi_g(1b_{2g})$	−6.97	82.85	1

Besides this, the data on DCS is further used to calculate the momentum-transfer cross section (MTCS) that shows the importance of backward angle scattering. Since the DCS are not very sensitive to correlation effects for backward scattering, we expect our MTCS to be quite reliable in 0.01–10 eV range. These are calculated in the one-state CI model with spin averaging. The MTCS provides a useful input in solving the Boltzmann equation for the electron distribution function. In contrast to the diverging nature of DCS in the forward direction, MTCSs show no singularity due to the weighting factor $(1-\cos\theta)$, where θ is scattering angle. This factor vanishes as $\theta \to 0$. The MTCS is useful in the study of electrons drifting through a molecular gas. When a swarm of electrons travel through a molecular gas under the influence of an electric field, several transport observables, such as diffusion coefficient D and mobility μ, can be obtained if we have a knowledge of the momentum-transfer cross sections. In Fig. 7, we have shown the calculated MTCSs at different energies for electron collision with a O_2 molecule and compared with previous data [12,15].

F. Effective collision frequency of electrons

The effective electron-neutral collision frequency $\langle v\rangle$, which is averaged over a Maxwellian distribution can be obtained from the momentum transfer cross section $Q^{(m)}(v)$ as follows [40]:

$$\langle v\rangle = \frac{8}{3\pi^{1/2}} N \left(\frac{m_e}{2kT_e}\right)^{5/2} \int_0^\infty v^5 Q^{(m)}(v) \exp\left(\frac{-m_e v^2}{2kT_e}\right) dv, \tag{8}$$

where m_e and T_e are the electron mass and temperature, respectively, k is Boltzmann's constant, v is the velocity, and N is the number density of the gas particles. The averaging is over a Maxwellian speed distribution function for an electron temperature T_e which is given by:

$$f(v) = 4\pi v^2 \left(\frac{m_e}{2\pi kT_e}\right)^{3/2} \exp\left(\frac{-m_e v^2}{2kT_e}\right). \tag{9}$$

This type of collision frequency is often used to evaluate the energy transfer between particles. Alternatively, the effective collision frequency for electrons can be defined from the DC conductivity as follows [41], [40]:

$$\bar{\nu}^{-1} = \frac{8}{3\pi^{1/2}N} \left(\frac{m_e}{2kT_e}\right)^{5/2} \int_0^\infty \frac{v^3}{Q^{(m)}(v)} \exp\left(\frac{-m_e v^2}{2kT_e}\right) dv. \tag{10}$$

This explicit form of effective collision frequency $\bar{\nu}$ is related to the drift velocity of electrons in a gas, insofar as a Maxwell distribution can be assumed. When $Q^{(m)}(v)$ is proportional to v^{-1}, the two effective collision frequencies, $\langle v\rangle$ and $\bar{\nu}$ agree. In Fig. 8, we have shown both types of effective collision frequencies as a function of electron temperature. It is to be noted that $\langle v\rangle$ lies higher than $\bar{\nu}$ in the entire electron temperature range.

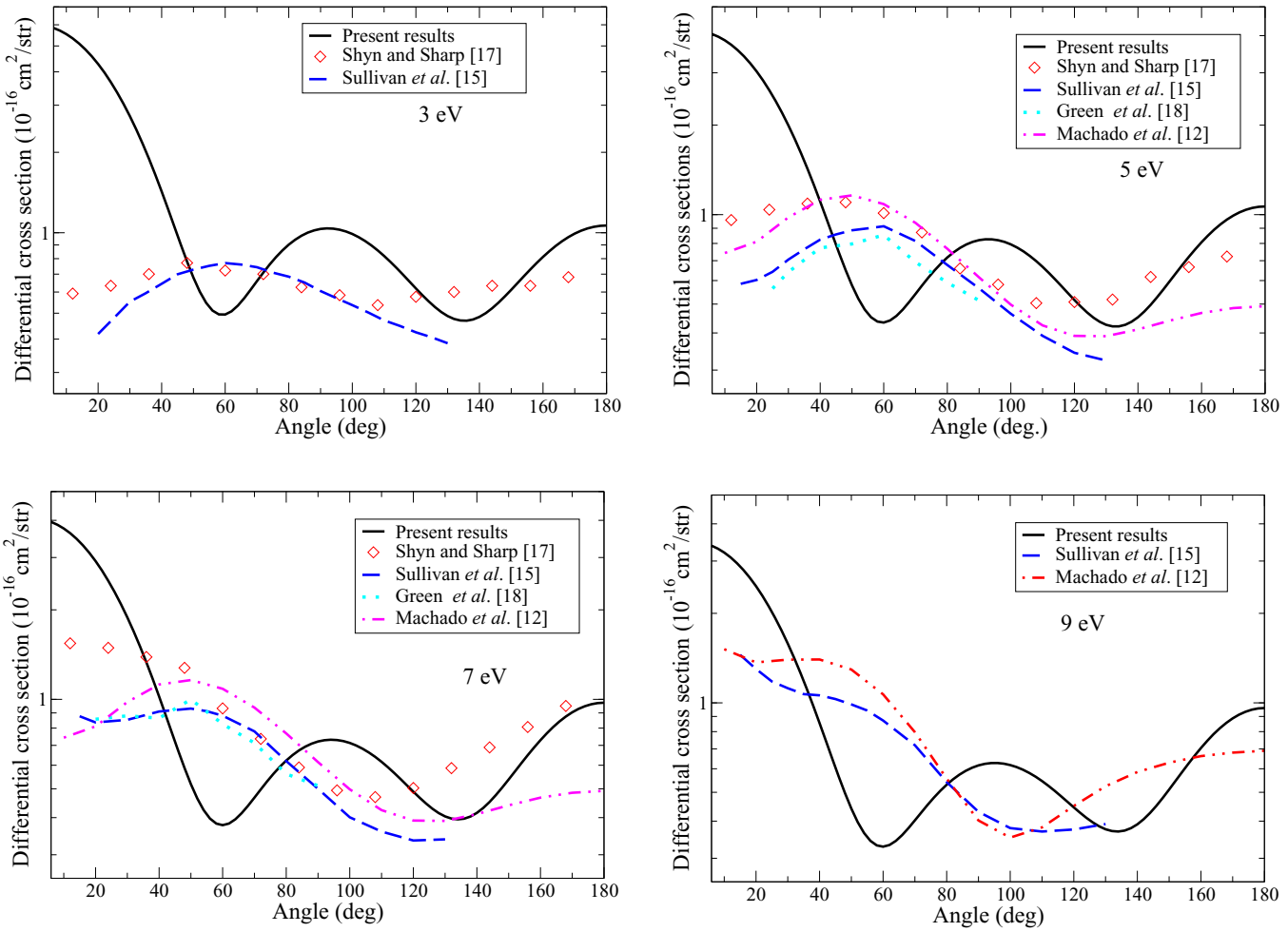

FIG. 6. (Color online) Differential cross sections (DCS) at 3 eV, 5 eV, 7 eV, and 9 eV for one-state CI model at R_e. red diamonds, Shyn and Sharp [17]; dashed blue curve, Sullivan *et al.* [15]; dotted cyan curve, Green *et al.* [18]; dash double-dotted magenta curve, Machado *et al.* [12]; solid black line, present results.

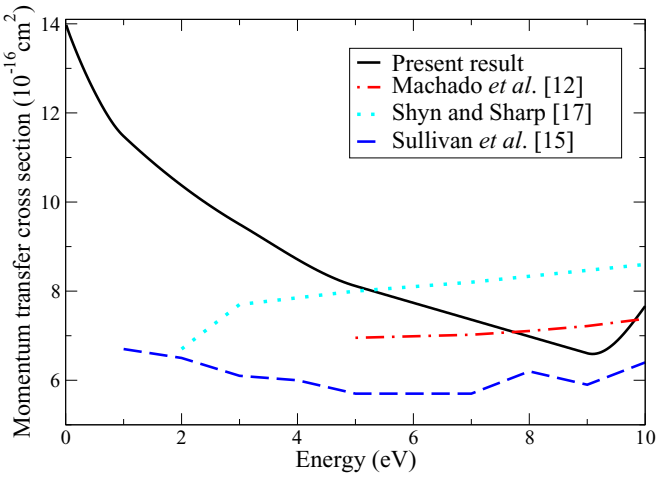

FIG. 7. (Color online) Momentum-transfer cross sections (MTCSs), at different energies, with spin average of O_2 molecule ground state at one-state CI level. dash-dotted red curve, Machado *et al.* [12]; dotted cyan curve, Shyn and Sharp [17]; dashed blue curve, Sullivan *et al.* [15]; solid black line, present results.

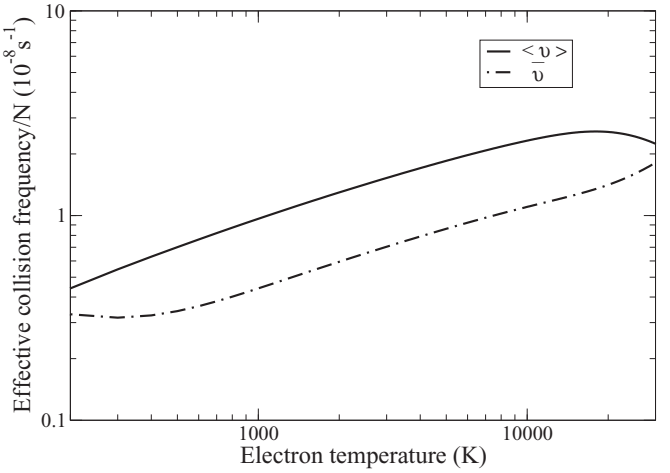

FIG. 8. Effective collision frequency as a function of electron temperature; dashed curve, $\bar{v}$; solid curve, $\langle v \rangle$.

G. Scattering length

We have also evaluated scattering length in our study of electron impact on the O_2 molecule. In this procedure we have included only an s-wave approximation for the scattering electron. The scattering length is given by

$$a = \frac{-\tan\delta_0}{k}, \quad k \to 0, \tag{11}$$

where, δ_0 is the eigenphase sum corresponding to the energy ($E = 0$). In practice, we have chosen $E = 0.025$ eV to compute a. Here k is the wave number of the scattering electron.

We have calculated of scattering length separately for doublets (a_D) and quartets (a_Q); the spin-averaged scattering length is given by

$$a = \left[\tfrac{1}{3}\left(a_D^2 + 2a_Q^2\right)\right]^{1/2}. \tag{12}$$

We obtained a value of 1.989 a_0 for the scattering length. Then we evaluated the cross section $\sigma = 4\pi a^2$ corresponding to this scattering length, which is equal to 49.687 ${a_0}^2$, this result is comparable with the cross section 49.535 ${a_0}^2$ at the same energy ($E = 0.025$ eV) coming from the direct calculation (R-matrix method).

IV. CONCLUSIONS

The significant advance made in the present work is the inclusion of greater polarization effect as compared to the previous work [10] by including 22 target states giving rise to stronger attractive interaction. This results in rather sharp $^2\Pi_u$ resonances in the excitation cross section of the a and b states of the O_2 molecule (Figs. 1 and 2). These appeared only very weakly and at considerably higher energy in previous work. This is due to better representation of the polarization effect in our calculations. This enhanced polarization is also responsible for the disappearance of shape resonance at a lower bond length $R = 3.6\, a_o$ than the previous work.

[1] T. G. Slanger, Science **265**, 1817 (1994).
[2] A. G. Middleton, M. J. Brunger, P. J. O. Teubner, M. W. B. Anderson, C. J. Noble, G. Woste, K. Blum, P. G. Burke, and C. Fullerton, J. Phys. B **27**, 4057 (1994).
[3] M. A. Khakoo, W. R. Newell, and A. C. H. Smith, J. Phys. B: At. Mol. Phys. **16**, L317 (1983).
[4] G. Herzberg, *Spectra of Diatomic Molecules*, Vol. I (Van Nostrand, Princeton, 1950), 2nd ed.
[5] A. D. Tait, M. Dixon, and K. E. Banyard, J. Phys. B **7**, 1908 (1974).
[6] B. J. Moss and W. A. Goddard, J. Chem. Phys. **63**, 3523 (1975).
[7] N. H. F. Beebe, E. W. Thulstrup, and A. Andersen, J. Chem. Phys. **64**, 2080 (1976).
[8] R. P. Saxon and B. Liu, J. Chem. Phys. **67**, 5432 (1977).
[9] D. Teillet-Billy, L. Malegat, and J. P. Gauyacq, J. Phys. B: At. Mol. Phys. **20**, 3201 (1987).
[10] C. J. Noble, P. G. Burke Phys. Rev. Lett. **68**, 2011 (1992).
[11] K. Higgins, C. J. Noble, and P. G. Burke, J. Phys. B: At. Mol. Opt. Phys. **27**, 3203 (1994).
[12] L. E. Machado, E. M. S. Ribeiro, M.-T. Lee, M. M. Fujimoto, and L. M. Brescansin, Phys. Rev. A **60**, 1199 (1999).
[13] K. N. Joshipura, B. K. Antony, and M. Vinodkumar, J. Phys. B: At. Mol. Opt. Phys. **35**, 4211 (2002).
[14] E. Krishnakumar and S. K. Srivastava, Int. J. Mass Spectrom. Ion Processes **113**, 1 (1992).
[15] J. P. Sullivan, J. C. Gibson, R. J. Gulley, and S. J. Buckman, J. Phys. B: At. Mol. Opt. Phys. **28**, 4319 (1995).
[16] G. Woste, C. J. Noble, K. Higgins, P. G. Burke, M. J. Brunger, P. J. O. Teubner, and A. G. Middleton, J. Phys. B: At. Mol. Opt. Phys. **28**, 4141 (1995).
[17] T. W. Shyn and W. E. Sharp, Phys. Rev. A **26**, 1369 (1982).
[18] M. A. Green, P. J. O. Teubner, B. Mojarrabi, and M. J. Brunger, J. Phys. B: At. Mol. Opt. Phys. **30**, 1813 (1997).
[19] L. A. Morgan, C. J. Gillan, J. Tennyson, and X. Chen, J. Phys. B: At. Mol. Opt. Phys. **30**, 4087 (1997).
[20] L. A. Morgan, J. Tennyson, and C. J. Gillan, Comput. Phys. Commun. **114**, 120 (1998).
[21] J. Tennyson, J. Phys. B: At. Mol. Opt. Phys. **29**, 1817 (1996).
[22] Y. K. Kim and M. E. Rudd, Phys. Rev. A **50**, 3954 (1994).
[23] W. Hwang, Y. K. Kim, and M. E. Rudd, J. Chem. Phys. **104**, 2956 (1996).
[24] J. Tennyson, Phys. Rep. **491**, 29 (2010).
[25] P. G. Burke, *R-Matrix Theory of Atomic Collisions: Application to Atomic, Molecular and Optical Processes* (Springer, Berlin, 2011).
[26] P. G. Burke and K. A. Berrington, *Atomic and Molecular Processes: an R-matrix Approach* (Institute of Physics Publishing, Bristol, 1993).
[27] C. J. Gillan, J. Tennyson, and P. G. Burke, *Computational Methods for Electron-Molecule Collisions*, edited by W M Huo and F A Gianturco (Plenum, New York, 1995).
[28] K. L. Baluja, P. G. Burke, and L. A. Morgan, Comput. Phys. Commun. **27**, 299 (1982).
[29] L. A. Morgan, Comput. Phys. Commun. **31**, 419 (1984).
[30] B. M. Nestmann, K. Pfingst, and S. D. Peyerimhoff, J. Phys. B: At. Mol. Opt. Phys. **27**, 2297 (1994).
[31] J. Tennyson, J. Phys. B: At. Mol. Opt. Phys. **29**, 6185 (1996).
[32] A. Faure, J. D. Gorfinkiel, L. A. Morgan, and J. Tennyson, Comput. Phys. Commun. **144**, 224 (2002).
[33] T. H. Dunning and P. J. Hay, *Methods of Electronic Structure Theory*, Vol. 2, edited by H. F. Schaefer (Plenum, New York, 1977).
[34] R. Gonzalez-Luque, M. Manuela, M. P. Fulscher, and B. O. Roos, Chem. Phys. Lett. **204**, 323 (1993).
[35] M. J. Travers, D. C. Cowless, and G. B. Ellison, Chem. Phys. Lett. **164**, 449 (1989).
[36] NIST, Phys Ref Data. http://physics.nist.gov/PhysRefData/Ionization
[37] E. S. Chang and A. Temkin, Phys. Rev. Lett. **23**, 399 (1969).
[38] F. A. Gainturco and A. Jain, Phys. Rep. **143**, 347 (1986).
[39] N. Sanna and F. A. Gianturco, Comput. Phys. Commun. **114**, 142 (1998).
[40] Y. Itikawa, Phys. Fluids **16**, 831 (1973).
[41] I. P. Shkarofsky, Can. J. Phys. **39**, 1619 (1961).